Fuel 206 (2017) 572–579

Contents lists available at ScienceDirect

Fuel

journal homepage: www.elsevier.com/locate/fuel

Full length article

Modelling heat of reaction in biomass pyrolysis with detailed reaction schemes

Andrés Anca-Couce [a,*], Robert Scharler [a,b]

[a] Institute of Thermal Engineering, Graz University of Technology, Inffeldgasse 25b, 8010 Graz, Austria
[b] BIOENERGY 2020+ GmbH, Inffeldgasse 21b, 8010 Graz, Austria

HIGHLIGHTS

- Calculation of biomass pyrolysis heat of reaction with a detailed reaction scheme.
- Inclusion of primary devolatilization and exothermic heterogeneous secondary charring.
- Description of heat evolution in micro-TGA-DSC experiments with and without a lid.
- Description of exothermic peak in single particle experiments.

ARTICLE INFO

Article history:
Received 24 October 2016
Received in revised form 3 May 2017
Accepted 1 June 2017

Keywords:
Biomass pyrolysis
Heat of reaction
Detailed reaction scheme
Modelling
Single particle
Exothermicity

ABSTRACT

Primary devolatilization and the exothermic heterogeneous secondary charring of the primary volatiles need to be described in a consistent manner in order to correctly predict the heat of reaction of biomass pyrolysis. Detailed reaction schemes can currently predict mass loss and product composition of biomass pyrolysis with good accuracy, but have a weakness in the description of the heat of reaction. In this work it is shown for the first time that including secondary charring reactions a detailed reaction scheme can predict the evolution of the heat of pyrolysis for different conditions. The enthalpy of reaction is calculated for each reaction as the difference between the net calorific value of reactants and products. The presented model is able to describe the heat evolution in micro-TGA-DSC experiments conducted without a lid, where pyrolysis is endothermic, and with a lid, where secondary reactions are enhanced and the global heat of reaction shifts to exothermic. Furthermore, when it is coupled to a particle model, it correctly describes single particle pyrolysis experiments conducted with beech spheres where there is a remarkably exothermic peak in the centre temperature.

1. Introduction

Biomass pyrolysis is a conversion process in which a thermal degradation takes place usually at temperatures in the range of 300–600 °C, producing a wide variety of products, including char, a pyrolytic liquid (liquid at room temperature, referred to as bio-oil or pyrolysis-oil) and permanent gases [1]. The products of biomass pyrolysis, mainly bio-oil [2] and bio-char [3], have plentiful applications. Pyrolysis has been proposed as a key technology in a bio-refinery concept [4], producing value-added chemicals, fuels, heat and power from biomass. Furthermore, pyrolysis is a main sub-process in other thermo-chemical processes such as combustion or gasification. Recent advances in the understanding of biomass pyrolysis have been reviewed by Anca-Couce [1]. Detailed reaction schemes which are able to describe the complex reactions that take place during biomass pyrolysis and can predict a detailed product composition are available in literature [5–7]. However, the heat of reaction of biomass pyrolysis remains a matter of controversy and up to date there is not available a model which can accurately predict it for different conditions.

The heat of reaction in experiments with small particle sizes (e.g. powder) can be determined by differential scanning calorimetry (DSC). Pyrolysis of woody biomass with samples of a few mg is commonly globally endothermic [8–10]. However, as shown by Rath et al. [8] and then reproduced by several authors [9,11,12], the exothermicity of the reaction significantly increases, as well as the char yield, when a lid is employed. The global reaction enthalpy can shift from endothermic to exothermic. The same effect is observed when a higher initial sample mass is employed or when experiments are conducted under higher pressure [13]. The opposite, a more endothermic reaction, is obtained when the

* Corresponding author.
E-mail address: anca-couce@tugraz.at (A. Anca-Couce).

http://dx.doi.org/10.1016/j.fuel.2017.06.011
0016-2361/

samples are previously washed in order to reduce the content of inorganics [9]. In all these DSC experiments exothermicity is enhanced when the extent of heterogeneous secondary charring reactions of the volatiles of biomass pyrolysis is increased, due to a higher retention time of the volatiles, pressure or presence of inorganics which can catalyse these reactions.

An exothermic behaviour has also been observed in single particle [14,15] and fixed-bed reactor [16,17] experiments. Three different zones have been identified: an initial exothermic peak, linked to hemicellulose, followed by an endothermic peak, linked to cellulose, and finally an exothermic peak, linked to lignin. Furthermore, exothermicity has also been observed in torrefaction experiments, where mainly hemicellulose decomposes [18,19]. Exothermicity during biomass pyrolysis has been recently reviewed by Di Blasi et al. [20], showing that it can produce thermal runaways of more than 100 °C. Although different interpretations are available in the literature, recent reviews show that exothermicity is linked with the heterogeneous secondary reactions of the volatiles [1,20], which also lead to the generation of (secondary) char. Evidences that support this interpretation are the previously described DSC experiments or the single particle experiments presented by Zobel and Anca-Couce [15], where Laser Induced Fluorescence (LIF) measurements of the volatiles evolving from a wood particle show that the production of polycyclic aromatic hydrocarbons (PAH) in charring reactions is correlated with a more exothermic heat of reaction.

Biomass pyrolysis is commonly modelled with a heat of reaction equal to zero or with slightly endothermic values, such as in the reference work of Gronli and Melaaen [21]. Corbetta et al. [6] proposed constant values for the enthalpy of the different reactions of a detailed reaction scheme. However, the reaction enthalpy can be significantly different, as previously discussed. The objective of this work is to present for the first time a detailed reaction scheme for biomass pyrolysis which can accurately predict the different heats of reaction that are obtained during biomass pyrolysis at different conditions. This model will be first validated with DSC experiments with different extents of secondary reactions and then applied in order to predict the exothermic behaviour experimentally detected in single particle experiments.

2. Models

2.1. Detailed reaction scheme

The detailed reaction scheme that is going to be employed is based on the one developed by Ranzi et al. [5] for primary pyrolysis. In this scheme biomass consists of cellulose, hemicellulose and 3 types of lignin which independently decompose and the volatiles are represented by several species, including main permanent gases and condensable species. This scheme has been adapted by Anca-Couce et al. [7,22] in order to consider the presence of heterogeneous secondary charring reactions during the pyrolysis process (not to be confused with the homogeneous tar cracking which can take place at higher temperatures in the gas phase). In these reactions char is produced together with other products, such as H_2O, CO_2 and H_2, from the primary products of biomass pyrolysis. This adapted scheme (RAC scheme), combining primary devolatilization and secondary charring, has been applied to describe the product composition of fixed-bed pyrolysis and torrefaction [7,22,23]. An update of the Ranzi scheme for primary pyrolysis has been presented by Corbetta et al. [6]. In this work, the heterogeneous secondary charring reactions are going to be introduced in the updated version of Corbetta et al. [6] as it has been previously done, so that an updated version of the RAC scheme is presented. The list of species is shown in Table 1 and the chemical reactions in Table 2. The modifications conducted in the adaptation are going to be summarized.

Table 1
List of species and calorific value.

Abbreviation	Name	Atomic composition	Net calorific value (kJ/g)
Solids			
CELL	Cellulose	$C_5H_8O_4$	16.32
CELLA	Activated cellulose	$C_5H_8O_4$	16.32
HCE	Hemicellulose	$C_5H_8O_4$	16.66
HCEHW	Hemicellulose (hardwoods)	$10*(C_5H_8O_4)+4*(C_2H_4O_2)$	16.38
HCESW	Hemicellulose (softwoods)	$10*(C_5H_8O_4)+(C_2H_4O_2)$	16.58
HCEA1	Activated hemicellulose 1	$C_5H_8O_4$	16.66
HCEA2	Activated hemicellulose 2	$C_5H_8O_4$	16.66
LIG-C	Carbon-rich lignin	$C_{15}H_{14}O_4$	26.99
LIG-H	Hydrogen-rich lignin	$C_{22}H_{28}O_9$	23.87
LIG-O	Oxygen-rich lignin	$C_{20}H_{22}O_{10}$	20.93
LIG-CC	Carbon-rich lignin 2	$C_{15}H_{14}O_4$	26.99
LIG-OH	OH-rich lignin	$C_{19}H_{22}O_8$	23.13
LIG	Intermediate lignin	$C_{11}H_{12}O_4$	24.50
G{CO_2}	Trapped CO_2	CO_2	0.0
G{CO}	Trapped CO	CO	10.11
G{COH_2}	Trapped COH_2	CH_2O	14.83
G{H_2}	Trapped H_2	H_2	95.78
G{CH_4}	Trapped CH_4	CH_4	50.13
G{CH_3OH}	Trapped CH_3OH	CH_4O	21.12
G{C_2H_4}	Trapped C_2H_4	C_2H_4	43.61
Char	Char	C	32.79
Volatiles			
HAA/AA	Hydroxyacetaldehyde/ Acetic acid	$C_2H_4O_2$	16.05
HCOOH	Formic acid	CH_2O_2	5.58
GLYOX	Glyoxal	$C_2H_2O_2$	14.09
C_3H_6O	Propanal (Acetone)	C_3H_6O	29.61
$C_3H_4O_2$	Propanedial	$C_3H_4O_2$	19.29
HMFU	5-hydroxymethyl-furfural	$C_6H_6O_3$	21.85
LVG	Levoglucosan	$C_6H_{10}O_5$	16.85
XYL	Xylose monomer	$C_5H_8O_4$	17.43
pCOUMARYL	Paracoumaryl alcohol	$C_9H_{10}O_2$	30.28
PHENOL	Phenol	C_6H_6O	31.72
FE2MACR	Sinapaldehyde	$C_{11}H_{12}O_4$	25.45
H_2	Hydrogen	H_2	120.9
CO	Carbon monoxide	CO	10.11
CO_2	Carbon dioxide	CO_2	0.0
CH_4	Methane	CH_4	50.14
CH_2O	Formaldehyde	CH_2O	17.31
CH_3OH	Methanol	CH_4O	21.12
C_2H_4	Ethylene	C_2H_4	47.25
CH_3CHO	Acetaldehyde	C_2H_4O	25.10
ETOH	Ethanol	C_2H_6O	27.76
H_2O	Water vapour	H_2O	0.0

Secondary charring reactions are introduced in reactions R2 and R3 for cellulose; R6, R7, R8 and R9 for hemicellulose; R13, R15, R16 and R17 for lignin and R19 and R23 for the G{} forms. R4 is not considered as charring is already introduced in R2 and R3 for cellulose. Adjustable parameters (x_{CELL}, x_{HCE}, x_{LIG} and $x_{G\{\}}$) represent the amount of primary products that react to produce the secondary products. The product composition of secondary reactions is selected as explained in [7]. The G{} forms presented in the scheme of Corbetta et al. [6], which represent volatiles trapped within a metaplastic phase, can be classified in low temperature G{} forms (G{CO}, G{CO_2} and G{CH_3OH}), released after the main devolatilization peak at temperatures around 400–600 °C, and high temperature G{} forms (G{COH_2}, G{H_2}, G{CH_4} and G{C_2H_4}), released at temperatures higher than 700 °C. Secondary charring reactions have also been considered for the low temperature G{} forms with an elemental composition which can lead to char and

Table 2
List of reactions of the updated RAC scheme (SW: softwood, HW: hardwood).

	Reaction	A [s^{-1}]	E [kJ/mol]	Δh [kJ/g]
1	CELL → CELLA	4×10^{13}	188.37	0.0
2	CELLA → $(1 - x_{CELL})$ * (0.45 HAA + 0.2 GLYOX + 0.3 C_3H_6O + 0.25 HMFU + 0.05 H_2 + 0.31 CO + 0.41 CO_2 + 0.4 CH_2O + 0.15 CH_3OH + 0.1 CH_3CHO + 0.83 H_2O + 0.02 HCOOH + 0.05 G{H_2} + 0.2 G{CH_4} + 0.61 Char) + x_{CELL} * (5.5 Char + 4 H_2O + 0.5 CO_2 + H_2)	2×10^{6}	80.0	0.56 $(1 - x_{CELL})$ − 1.47 x_{CELL}
3	CELLA → $(1 - x_{CELL})$ * (LVG/same products as R2) + x_{CELL} * (5.5 Char + 4 H_2O + 0.5 CO_2 + H_2)	$4 \times T$	41.86	0.53 $(1 - x_{CELL})$ − 1.47 x_{CELL}
4	Not included			
5	HCE → 0.4 AA (HW)/0.1 AA (SW) + 0.58 HCEA1 + 0.42 HCEA2	1×10^{10}	129.77	0.0
6	HCEA1 → $(1 - x_{HCE})$ * (0.5 CO + 0.5 CO_2 + 0.325 CH_4 + 0.8 CH_2O + 0.1 CH_3OH + 0.25 C_2H_4 + 0.125 ETOH + 0.025 H_2O + 0.025 HCOOH + 0.275 G{CO_2} + 0.4 G{COH_2} + 0.125 G{H_2} + 0.45 G{CH_3OH} + 0.875 Char) + x_{HCE} * (4.5 Char + 3 H_2O + 0.5 CO_2 + H_2)	1.2×10^{9}	125.58	0.25 $(1 - x_{HCE})$ − 1.42 x_{HCE}
7	HCEA1 → $(1 - x_{HCE})$ * (0.1 CO + 0.8 CO_2 + 0.3 CH_2O + 0.25 H_2O + 0.05 HCOOH + 0.15 G{CO_2} + 0.15 G{CO} + 1.2 G{COH_2} + 0.2 G{H_2} + 0.625 G{CH_4} + 0.375 G{C_2H_4} + 0.875 Char) + x_{HCE} * (4.5 Char + 3 H_2O + 0.5 CO_2 + H_2)	$0.15 \times T$	33.5	−0.64 $(1 - x_{HCE})$ − 1.42 x_{HCE}
8	HCEA1 → $(1 - x_{HCE})$ * (XYL/same as R6) + x_{HCE} * (4.5 Char + 3 H_2O + 0.5 CO_2 + H_2)	$3 \times T$	46.05	0.77 $(1 - x_{HCE})$ − 1.42 x_{HCE}
9	HCEA2 → $(1 - x_{HCE})$ * (0.2 HAA + 0.175 CO + 0.275 CO_2 + 0.5 CH_2O + 0.1 ETOH + 0.2 H_2O + 0.025 HCOOH + 0.4 G{CO_2} + 0.925 G{COH_2} + 0.25 G{CH_4} + 0.3 G{CH_3OH} + 0.275 G{C_2H_4} + Char) + x_{HCE} * (4.5 Char + 3 H_2O + 0.5 CO_2 + H_2)	0.5×10^{10}	138.14	−0.14 $(1 - x_{HCE})$ − 1.42 x_{HCE}
10	LIG-C → 0.35 LIG-CC + 0.1 pCOUMARYL + 0.08 PHENOL + 0.32 CO + 0.3 CH_2O + H_2O + 0.7 G{COH_2} + 0.495 G{CH_4} + 0.41 G{C_2H_4} + 5.735 Char	1.33×10^{15}	203.02	−0.47
11	LIG-H → LIG-OH + 0.25 HAA + 0.5 C_3H_6O + 0.5 G{C_2H_4}	0.67×10^{13}	156.97	0.10
12	LIG-O → LIG-OH + CO_2	0.33×10^{9}	106.74	−0.21
13	LIG-CC → $(1 - x_{LIG})$ * (0.35 HAA + 0.3 pCOUMARYL + 0.2 PHENOL + 0.4 CO + 0.65 CH_4 + 0.6 C_2H_4 + 0.7 H_2O + 0.4 G{CO} + G{COH_2} + 6.75 Char) + x_{LIG} * (15 Char + 4 H_2O + 3 H_2)	3×10^{7}	131.86	−0.09 $(1 - x_{LIG})$ − 1.30 x_{LIG}
14	LIG-OH → LIG + 0.55 CO + 0.05 CO_2 + 0.1 CH_4 + 0.6 CH_3OH + 0.9 H_2O + 0.05 HCOOH + 0.6 G{CO} + 0.85 G{COH_2} + 0.1 G{H_2} + 0.35 {CH_4} + 0.3 G{CH_3OH} + 0.2 G{C_2H_4} + 4.15 Char	1×10^{8}	125.58	−0.17
15	LIG → $(1 - x_{LIG})$ * FE2MACR + x_{LIG} * (10.5 Char + 3 H_2O + 0.5 CO_2 + 3 H_2)	$4 \times T$	50.2	0.95 $(1 - x_{LIG})$ − 1.52 x_{LIG}
16	LIG → $(1 - x_{LIG})$ * (0.2 C_3H_6O + CO + 0.2 CH_4 + 0.2 CH_2O + 0.4 CH_3OH + 0.2 CH_3CHO + 0.95 H_2O + 0.05 HCOOH + 0.45 G{CO} + 0.5 G{COH_2} + 0.4 {CH_4} + 0.65 G{C_2H_4} + 5.5 Char) + x_{LIG} * (10.5 Char + 3 H_2O + 0.5 CO_2 + 3 H_2)	0.4×10^{9}	125.58	−0.35 $(1 - x_{LIG})$ − 1.52 x_{LIG}
17	LIG → $(1 - x_{LIG})$ * (0.4 CO + 0.2 CH_4 + 0.4 CH_2O + 0.6 H_2O + 0.2 G{CO} + 2 G{COH_2} + 0.4 {CH_4} + 0.4 G{CH_3OH} + 0.5 G{C_2H_4} + 6 Char) + x_{LIG} * (10.5 Char + 3 H_2O + 0.5 CO_2 + 3 H_2)	$0.083 \times T$	33.5	−0.50 $(1 - x_{LIG})$ − 1.52 x_{LIG}
18	G{CO_2} → CO_2	1×10^{5}	100.46	0.0
19	G{CO} → $(1 - x_{G\{\}})$ * CO + $x_{G\{\}}$ * (0.5 Char + 0.5 CO_2)	3×10^{13}	209.3	−3.08 $x_{G\{\}}$
20	G{COH_2} → 0.75 G2{COH_2} + 0.25 (H_2 + 0.5 CO + 0.25 CO_2 + 0.25 Char)	1×10^{6}	100.46	0.31
21	G{H_2} → H_2	1×10^{12}	313.96	0.0
22	G{CH_4} → CH_4	2×10^{13}	300.0	0.01
23	G{CH_3OH} → $(1 - x_{G\{\}})$ * CH_3OH + $x_{G\{\}}$ * (Char + H_2O + H_2)	1.2×10^{13}	209.3	−1.27 $x_{G\{\}}$
24	G{C_2H_4} → 0.3 C_2H_4 + 0.7 (CH_4 + Char)	1×10^{6}	100.46	0.46
25	G2{COH_2} → 0.2 G3{COH_2} + 0.8 (CO + H_2)	1.5×10^{9}	209.3	0.0

the other typical products of these reactions (H_2O, CO_2 and H_2), representing the condensation (bond-forming) reactions that take place after the degradation of biomass constituents [24].

The presence of alkali metals in biomass and heterogeneous secondary reactions lead to the preference of fragmentation over sugar formation for cellulose and hemicellulose. In reactions R3 and R8, depending on the case, the formation of the sugars LVG and XYL may be avoided and the fragmentation pathway (represented by reactions R2 and R6, respectively) be taken, as it will be described in section 3.1. Furthermore, the pre-exponential factor of reactions R13 (LIG-CC), R19 (G{CO}) and R23 (G{CH_3OH}) has been increased in order to improve the DSC results, as it will be explained in section 3.1. Moreover, in order to improve the predictions for the release of light hydrocarbons and char yield and composition in single particle experiments [25], it is considered that C_2H_4 is not released and it is trapped as G{C_2H_4} in reactions R10 (LIG-C) and R11 (LIG-H), while C_2H_4 and CH_4 are released (and not trapped as G{C_2H_4} and G{CH_4}) in reaction R13 (LIG-CC); the products of reactions R20 are modified, including G2{COH_2} which would further react at higher temperatures in reaction R25; the release of G{C_2H_4} in R24 produces CH_4 (and char), besides C_2H_4; and the kinetics of G{} forms reactions in R18, R20,

R21, R22, R24 and R25 have been as well modified. These modifications are discussed in detail in [25]. Finally, the release of acetic acid (AA) from hemicellulose is considered, including typical values for hardwoods and softwoods (SW), as explained in [22].

Besides, the net calorific value of the different species is shown in Table 1. These values will be employed in order to calculate the heat of reactions. The net calorific values of cellulose, hemicellulose and lignin solid species are calculated from the elemental composition of the model according to the correlation of Gaur [26]. This has also been done for the considered high temperature G{} forms in the scheme of Corbetta et al. [6], as the hydrogen and oxygen content in this solid material is embedded in the char graphite-like structure. On the other hand, known values are taken for the volatiles species, which are calculated from the enthalpy of formation in the gas phase at 25 °C from the ANSYS Fluent internal database. For the low temperature G{} forms, it is assumed that the heat of reaction for their release is zero. Furthermore, no heat of reaction is considered for reactions R21, R22 and R25, where high temperature G{} forms are released, as in this study the heat of reaction is compared with experiments conducted until final temperatures of around 500 °C and therefore it cannot be discussed for higher temperatures. The enthalpy of each reaction is shown in Table 2. For reactions R3 and R8 the values for the sugar formation pathways are shown. Moreover, the effect of temperature on heat of reaction has not been considered.

2.2. Single particle model

The single particle model is a one-dimensional volumetric model in which the single particle is discretized in control volumes. The main features of the model are that the properties are considered to be one dimensional in space and transient in time, there is local thermal equilibrium between the solid and the gas phase, the volatiles are considered as ideal gases, transport of mass occurs by convection and diffusion, heat transfer occurs by conduction, convection and radiation, shrinkage can be included and there is no fragmentation of the particle. Details of the model can be found in [27]. Pyrolysis has been previously described with the single component competitive scheme, which is a simple scheme, and it is replaced in this work by the detailed reaction scheme that has been presented in section 2.1.

3. Results and discussion

As it has been reviewed in Section 1, the presence of heterogeneous secondary charring reactions is linked with exothermicity during biomass pyrolysis. Therefore, a model which is able to describe the heat of reaction at different conditions should be able to predict the increase in exothermicity when secondary reactions are enhanced. The presented model in section 2.1 is going to be first applied for different components and values for "x" (x_{CELL}, x_{HCE}, x_{LIG} and $x_{G\{\}}$), representing the amount of secondary charring reactions. The heat of reaction (Δh) is calculated as the difference between the net calorific value of reactants and products, without considering the devolatilization of G{} forms. The results are shown in Fig. 1, where it can be seen that higher "x" values, i.e. more secondary charring reactions, result is a more exothermic process. This is because the net calorific value of secondary products (mainly char and water) is lower than the one of primary products of pyrolysis for all components. Furthermore, cellulose pyrolysis is more endothermic than hemicellulose and lignin pyrolysis. This shows the general suitability of the RAC scheme in order to describe the heat of reaction at different conditions. The results have been obtained considering that no sugars are produced in reactions R3 and R8 for cellulose and hemicellulose,

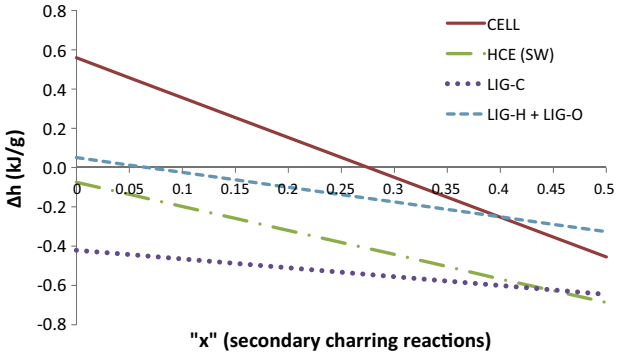

Fig. 1. Heat of reaction for different extents of secondary charring reactions with reference to the RAC scheme for different components. A typical softwood hemicellulose is considered.

respectively, and the fragmentation pathway is followed, as typically when secondary reactions are dominant. If sugars formation is considered in R3 and R8, the slope of the cellulose and hemicellulose lines in Fig. 1 would not be modified and Δh for "x" equal to zero (no secondary charring) would be equal to 0.537 kJ/g for cellulose and 0.084 kJ/g hemicellulose.

Furthermore, the char yield and enthalpy of the secondary reactions are shown in Table 3. It is reported in the literature that the heat of reaction is almost a linear function of the char yield, however the available values differ [16]. For cellulose, values of 3.6 [28], 2.0 [29] and 5.1 [30] kJ/g $_{char}$ have been reported. A value of 3.62 kJ/g $_{char}$ is obtained with the applied model, which is in the range of values reported in literature. Values for other components are not available in literature, while for biomass values of 3.5 and 3.8 kJ/g $_{char}$ for beech and spruce, respectively [8], and 0.9 kJ/g $_{char}$ for artichoke thistle [9] have been reported. The model predicts a similar value for hemicellulose than cellulose and lower values for lignin, although charring is also produced from the intermediate G{} forms, with high values due to the low char yield in these reactions. The values obtained by the model for biomass will be analysed in the next subsection. It should be as well noted that the influence of temperature on heat of reaction is not considered in this study, but as noted by Haseli et al. [31] its effect is minor in comparison to the endothermicity of devolatilization and exothermicity of charring. After showing the general suitability of the RAC model to predict the heat of reaction with different extents of secondary charring reactions, the model will be validated with DSC experiments in section 3.1 and then applied to predict an exothermic behaviour in single particle experiments in section 3.2.

3.1. DSC experiments

The model is going to be applied for the micro-TGA-DSC experiments presented by Rath et al. [8]. Experiments have been conducted with spruce wood with a heating rate of 10 K/min up to a temperature of 500 °C and initial masses ranging from 5 to 10 mg. The mass loss (TGA – thermo-gravimetric analysis) and heat of reaction (DSC) have been measured over time. TGA experiments have been conducted without a lid, as commonly done in literature, and with a lid, in order to increase the retention time of the volatiles in contact with the solid sample and, therefore, the secondary reactions. The RAC model is applied with a typical softwood composition – 44.0% CELL, 26.0 HCE, 17.5% LIG-C, 9.5% LIG-H, 3.0% LIG-O – and softwood hemicellulose (one molecule of acetic acid per 10 xylan molecules), as presented in [22]. Furthermore, the model will be applied with the parameters shown in Table 4. Two conditions will be considered, with a low a high charring. The parameters for low charring and high charring are applied

Table 3
Char yield and enthalpy of reaction in heterogeneous secondary reactions.

	Present in reaction	% char yield	Enthalpy of secondary charring	
			$kJ/g_{secondary\ products}$	kJ/g_{char}
CELL	R2, R3	40.74	−1.47	−3.62
HCE	R6, R7, R8, R9	40.91	−1.42	−3.47
LIG (from LIG-OH)	R15, R16, R17	60.57	−1.52	−2.51
LIG-CC	R13	69.77	−1.30	−1.65
G{CO}	R19	21.43	−3.08	−14.37
G{CH_3OH}	R23	37.5	−1.27	−3.37

Table 4
Detailed reaction scheme parameters.

	Low charring	High charring
X_CELL	0.025	0.1
X_HCE	0.05	0.2
X _LIG	0.075	0.3
X_G{}	0.1	0.4
Sugar formation in R3 and R8	Yes	No

in order to predict the experiments without and with a lid, respectively. The lowest "x" parameter is in the two cases for cellulose and progressively higher values are proposed for hemicellulose, lignin and G{} forms. This selection is based on literature, as it is known that the amount of charring increases in this order: cellulose, hemicellulose and lignin [1]. The values for the high charring conditions are four times higher than the ones for low charring. Furthermore, sugar formation in reactions R3 and R8 is avoided for the parameters set high charring, due to the high amount of secondary reactions which avoid the formation of these products, and considered for the low charring conditions.

The mass loss evolution is shown in Fig. 2. It can be seen that the RAC scheme can predict it with a very good accuracy. There are minor deviations in the final char yield, considering the limited reproducibility of this parameter in TGA experiments [8]. The solid yield is at 450 °C of 21.3 and 26.2% without and with lid in the experiments and of 23.3 and 29.9%, respectively, according to the model. In the reference work of Gronli et al. [32] a char yield at 500 °C of 22.9 ± 2.7% is obtained for typical TGA experiments (without lid) with 5 different softwood species. The model, for the low charring case, predicts a char yield at 500 °C of 20.3%, inside the standard deviation. Furthermore, the increase in the char yield is accurately predicted, with around 6% more when the lid is introduced (+5.9% in the experiments and +5.8% in the model at 500 °C).

The evolution of heat of reaction for the two conditions is shown in Fig. 3. In the experiment without lid a global endothermic heat of reaction is obtained, with a slight exothermic peak at the end. In the case with a lid, there is first an exothermic peak, attributed to hemicellulose, followed by an endothermic peak, attributed to cellulose, and finally an remarkable exothermic peak, attributed to lignin and G{} forms. The RAC scheme can predict the two cases with reasonable accuracy. In the case without lid there is an under-prediction of the endothermic area (see also Table 5), especially at the beginning of the experiment, while the final exothermic area is very well predicted. In the case with a lid, the

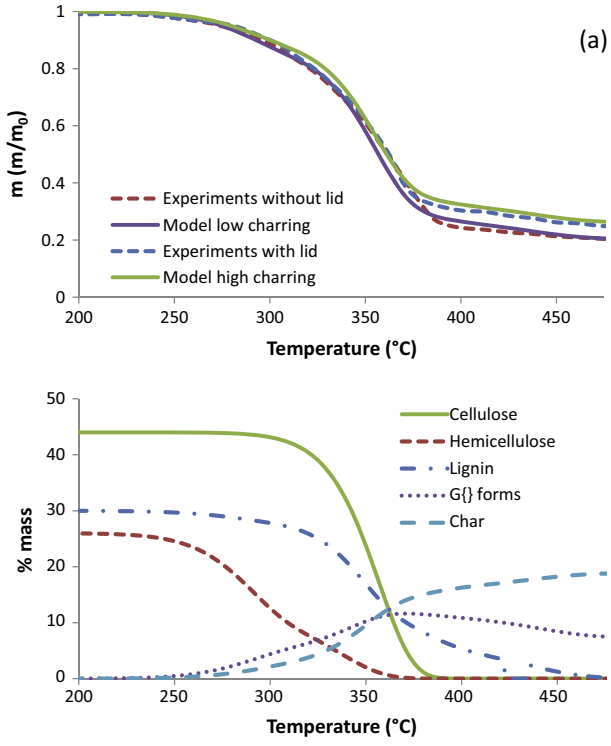

Fig. 2. Mass loss and model predictions in TGA-DSC experiments of Rath et al. [8] (a) and evolution of main solid components for the model high charring (b).

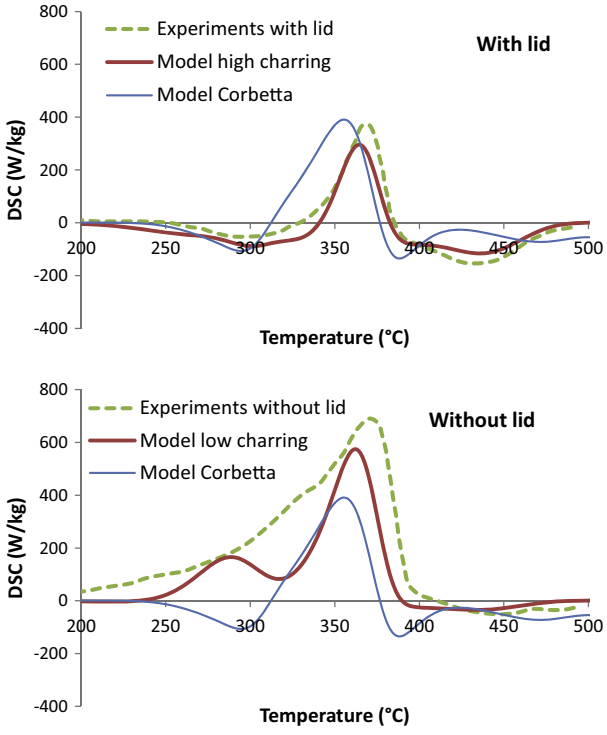

Fig. 3. Heat of reaction and model predictions in TGA-DSC experiments of Rath et al. [8].

Table 5
Heat of reactions of the different areas in DSC experiments.

	Without lid/Low charring		With lid/High charring	
	Experiments[8]	Model	Experiments[8]	Model
1st exothermic area (kJ/kg)	0	0	−10	−39
Endothermic area (kJ/kg)	315	169	42	41
2nd exothermic area (kJ/kg)	−25	−13	−51	−46
Total area (kJ/kg)	290	156	−19	−44

central endothermic area and the final exothermic area are very well predicted, while the first exothermic area is over-predicted. The overall predictions are good and the main divergences are present in the low temperature zone, where mainly hemicellulose decomposes. It should be noted that the pre-exponential factor of reactions R13, R19 and R23 (linked to LIG-CC and G{} forms) has been increased in order to accurately predict the position of the exothermic peak that takes place at high temperatures. Furthermore, comparing the difference in char yield and global heat of reaction between the two cases, the RAC model predicted an enthalpy of secondary charring reactions of −3.1 k/g $_{char}$ for softwood, which is in the range of reported values in literature. Finally, it is also shown in Fig. 3 the heat of reaction obtained with the application of the detailed scheme proposed by Corbetta et al. [6], which describes primary pyrolysis. It is shown that this scheme can predict some general aspects of the experiments, such as the endothermicity arising from cellulose pyrolysis at middle temperatures, but the deviations to experimental results are not minor and it is not able to describe the differences between the two experiments, as secondary charring is not introduced in that version of the scheme.

It has been already shown in previous works in literature that detailed reaction schemes are able to predict mass loss and product composition of biomass pyrolysis with a good accuracy. In this work it is also shown that they also are able to predict the heat of reaction in a consistent manner, provided that secondary charring reactions are considered. It should be noted that these DSC experiments could be modelled with variations only in the adjustable parameters shown in Table 4. The employed "x" values for low charring conditions are valid for typical micro-TGA experiments (without lid), where pyrolysis of woody biomass is endothermic. It is to be expected that similar values would also be valid for typical fast pyrolysis conditions, with a low charring and also endothermic [2] and for which micro-TGA conditions can be representative [33], but this should be confirmed in future work. The higher "x" values, employed for high charring conditions, would be valid for typical slow pyrolysis experiments with particles of a certain size, such as in typical fixed bed conditions, where exothermicity has been measured, especially at the end of the experiment.

3.2. Single particle experiments

In this section it will be shown that the RAC scheme can predict the exothermic peaks that are reported in literature for pyrolysis of thick wood particles. For this purpose, the single particle experiments conducted by Park et al. [14] will be modelled. The experiments have been conducted with dry beech wood spheres with a diameter of 25.4 mm that have been pyrolyzed at different temperatures, measuring the mass loss and temperatures at different positions. The single particle model described in section 2.2 has been applied with a spherical discretization. The model properties are taken from Park et al. [14] and are stated in Table 6. Shrinkage is not described, the calculation of the thermal conductivity in the solid phase includes radiation, as in [27], and the external boundary condition for the energy equation describes heat transfer by radiation and convection. The RAC pyrolysis model is applied with a typical hardwood composition – 44.0% CELL, 34.0 HCE, 6.0% LIG-C, 7.0% LIG-H, 9.0% LIG-O – and hardwood hemicellulose (four molecules of acetic acid per 10 xylan molecules) [22]. The parameters for the high charring conditions in Table 4 are selected for this case.

Table 6
Single particle model properties.

Property	Value	Unit
Density wood	1500	kg/m^3
Density char	1500	kg/m^3
Initial porosity	0.58	–
Heat capacity wood	1500 + T	J/(kg * K)
Heat capacity char	420 + 2.09 * T − 6.85·10^{-4} * T^2	J/(kg * K)
Heat capacity moisture	4200	J/(kg * K)
Thermal conductivity wood	0.2	W/(m * K)
Thermal conductivity char	0.1	W/(m * K)
Thermal conductivity gas	0.0258	W/(m * K)
Permeability wood	5·10^{-16}	m^2
Permeability char	1·10^{-13}	m^2
Pore diameter	1·10^{-4}	m
Emissivity	0.8	–
Viscosity gas	3·10^{-5}	kg/(m * s)
External heat transfer coefficient (α)	20	W/(m^2 * K)
Initial temperature	300	K

The experiments conducted with external temperatures of 415 °C and 463 °C have been simulated, where the exothermic peaks are clearly seen. Other experiments at higher temperatures are not considered, as homogeneous tar cracking in the gas phase may be relevant (according to literature, it is relevant for temperatures higher than 500 °C [1]). The results regarding mass loss and temperature evolution of the surface and the center of the particle are presented in Fig. 4. It can be seen that very good predictions are obtained with the applied models. The slight exothermic peak in the experiment at 415 °C and the more remarkable peak in the experiment at 463 °C are predicted with a good accuracy. This is also the case for the plateau in the center temperature before the final peak, which arises from the endothermicity of cellulose pyrolysis, when hemicellulose pyrolysis (exothermic in this case) is over.

It has been shown that the model is able to correctly describe the variations of the heat of reaction that take place during single particle experiments. Previous pyrolysis models coupled with particle models, such as the one presented in the work of Park et al. [14] or the latest version of the model of Ranzi [6], are only valid for the particular case for which they have been fitted, but will not have a general applicability as this one. For this purpose, it is needed a pyrolysis model which describes the endothermic primary devolatilization, mainly endothermic, and the exothermic secondary charring, as it is done in this work for the first time with a detailed reaction scheme.

The model has however some limitations. The "x" parameters have to be determined a priori and no correlations are available

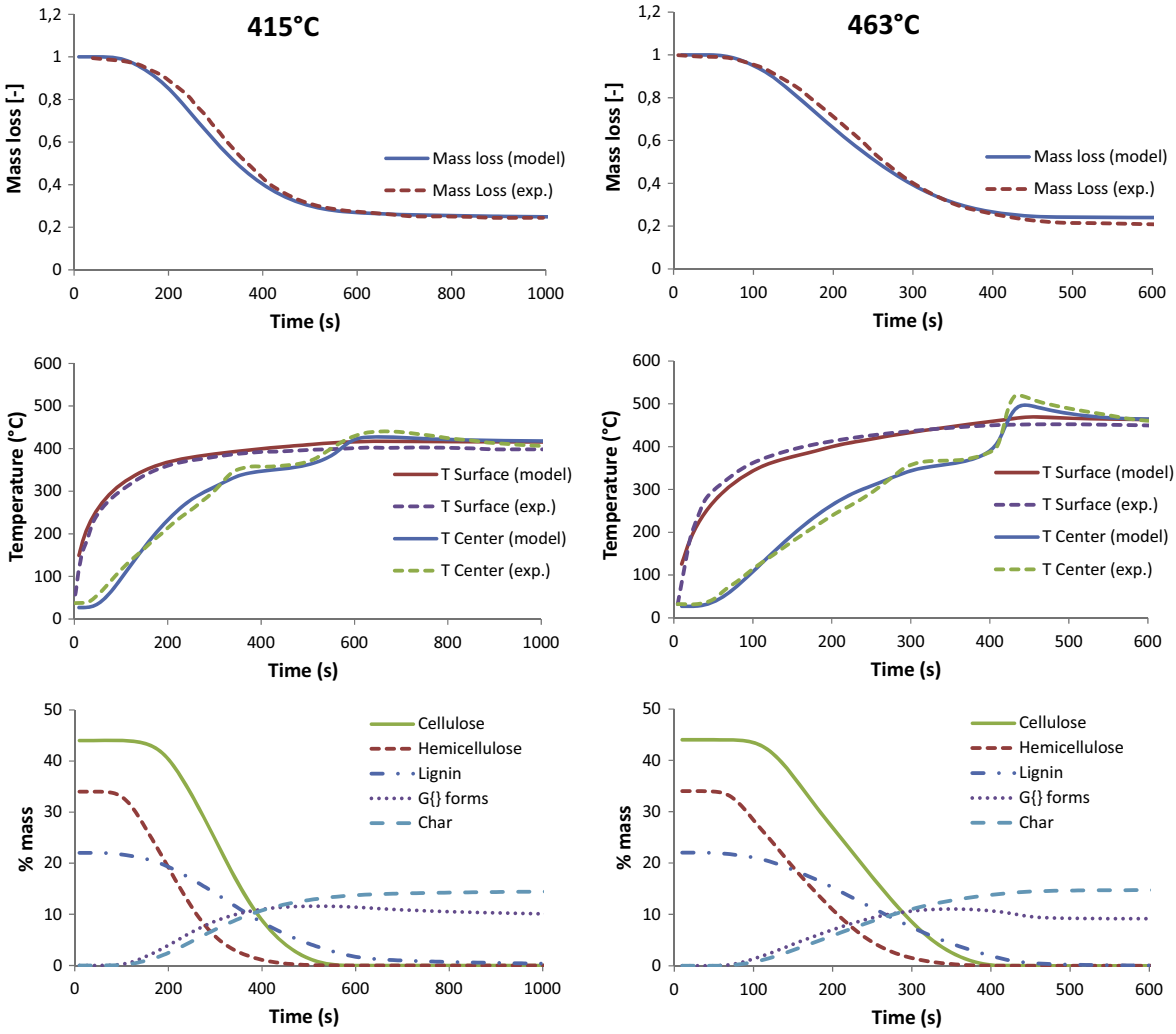

Fig. 4. Mass loss, temperatures and evolution of main solid components according to the model for the single particle experiments of Park et al. [14] at 415 °C (left) and 463 °C (right).

to determine the influence of parameters such as heating rate, particle size or other ones which could influence the heat of reaction, such as a higher ash content or pressure [20,13]. Future work should aim at the independent description of secondary heterogeneous charring reactions, separated from primary devolatization reactions, so that these secondary reactions are calculated as a function of temperature, retention time of volatiles, pressure and possible influence of catalysts.

4. Conclusions

The heat of reaction during biomass pyrolysis has been for the first time consistently described with a detailed reaction scheme, where the primary devolatilization and the exothermic heterogeneous secondary charring of the primary volatiles are included. The presented model is able to describe the heat evolution in micro-TGA-DSC experiments conducted without a lid, where pyrolysis is endothermic, and with a lid, where secondary reactions are enhanced and the global heat of reaction shifts to exothermic. Furthermore, when it is coupled to a particle model, it correctly describes single particle pyrolysis experiments conducted with beech spheres where there is a remarkably exothermic peak in the centre temperature. Future work should aim at the calculation of the amount of secondary charring reactions as a function of the process parameters, avoiding an a priori determination.

References

[1] Anca-Couce A. Reaction mechanisms and multi-scale modelling of lignocellulosic biomass pyrolysis. Prog Energy Combust Sci 2016;53:41–79.
[2] Bridgwater AV. Upgrading biomass fast pyrolysis liquids. Environ Prog Sustainable Energy 2012;31(2):261–8.
[3] Manya JJ. Pyrolysis for biochar purposes: a review to establish current knowledge gaps and research needs. Environ Sci Technol 2012;46 (15):7939–54.
[4] Balat M, Balat M, Kirtay E, Balat H. Main routes for the thermo-conversion of biomass into fuels and chemicals. Part 1: Pyrolysis systems. Energy Convers Manage 2009;50(12):3147–57.
[5] Ranzi E, Cuoci A, Faravelli T, Frassoldati A, Migliavacca G, Pierucci S, et al. Chemical kinetics of biomass pyrolysis. Energy Fuels 2008;22(6):4292–300.
[6] Corbetta M, Frassoldati A, Bennadji H, Smith K, Serapiglia MJ, Gauthier G, et al. Pyrolysis of centimeter-scale woody biomass particles: kinetic modeling and experimental validation. Energy Fuels 2014;28(6):3884–98.
[7] Anca-Couce A, Mehrabian R, Scharler R, Obernberger I. Kinetic scheme of biomass pyrolysis considering secondary charring reactions. Energy Convers Manage 2014;87:687–96.
[8] Rath J, Wolfinger MG, Steiner G, Krammer G, Barontini F, Cozzani V. Heat of wood pyrolysis. Fuel 2003;82(1):81–91.
[9] Gomez C, Velo E, Barontini F, Cozzani V. Influence of secondary reactions on the heat of pyrolysis of biomass. Ind Eng Chem Res 2009;48(23):10222–33.
[10] Anca-Couce A, Zobel N, Berger A, Behrendt F. Smouldering of pine wood: kinetics and reaction heats. Combust Flame 2012;159(4):1708–19.

[11] Manya JJ, Laguarta S, Ortigosa MA. Study on the biochar yield and heat required during pyrolysis of two-phase olive mill waste. Energy Fuels 2013;27(10):5931–9.
[12] Chen Q, Yang RM, Zhao B, Li Y, Wang SJ, Wu HW, et al. Investigation of heat of biomass pyrolysis and secondary reactions by simultaneous thermogravimetry and differential scanning calorimetry. Fuel 2014;134:467–76.
[13] Basile L, Tugnoli A, Stramigioli C, Cozzani V. Influence of pressure on the heat of biomass pyrolysis. Fuel 2014;137:277–84.
[14] Park WC, Atreya A, Baum HR. Experimental and theoretical investigation of heat and mass transfer processes during wood pyrolysis. Combust Flame 2010;157(3):481–94.
[15] Zobel N, Anca-Couce A. Influence of intraparticle secondary heterogeneous reactions on the reaction enthalpy of wood pyrolysis. J Anal Appl Pyrol 2015;116:281–6.
[16] Di Blasi C, Branca C, Masotta F, De Biase E. Experimental analysis of reaction heat effects during beech wood pyrolysis. Energy Fuels 2013;27(5):2665–74.
[17] Di Blasi C, Branca C, Sarnataro FE, Gallo A. Thermal runaway in the pyrolysis of some lignocellulosic biomasses. Energy Fuels 2014;28(4):2684–96.
[18] Turner I, Rousset P, Remond R, Perre P. An experimental and theoretical investigation of the thermal treatment of wood (Fagus sylvatica L.) in the range 200–260 degrees C. Int J Heat Mass Transf 2010;53(4):715–25.
[19] Bates RB, Ghoniem AF. Modeling kinetics-transport interactions during biomass torrefaction: the effects of temperature, particle size, and moisture content. Fuel 2014;137:216–29.
[20] Di Blasi C, Branca C, Galgano A. On the experimental evidence of exothermicity in wood and biomass pyrolysis. Energy Technol 2017;5:19–29.
[21] Gronli MG, Melaaen MC. Mathematical model for wood pyrolysis – comparison of experimental measurements with model predictions. Energy Fuels 2000;14(4):791–800.
[22] Anca-Couce A, Obernberger I. Application of a detailed biomass pyrolysis kinetic scheme to hardwood and softwood torrefaction. Fuel 2016;167:158–67.
[23] Anca-Couce A, Mehrabian R, Scharler R, Obernberger I. Kinetic scheme to predict product composition of biomass torrefaction. Chem Eng Trans 2014;37:43–8.
[24] Hasan MDM, Hu X, Gunawan R, Li CZ. Pyrolysis of large mallee wood particles: temperature gradients within a pyrolysing particle and effects of moisture content. Fuel Process Technol 2017;158:163–71.
[25] Anca-Couce A, Sommersacher P, Scharler R. Online experiments and modelling with a detailed reaction scheme of single particle biomass pyrolysis. J Anal Appl Pyrol 2017 [in review].
[26] Gaur S, Reed T. An atlas of thermal data for biomass and other fuels. Golden, Colorado, USA: Technical report at: National Renewable Energy Laboratory; 1995.
[27] Anca-Couce A, Zobel N. Numerical analysis of a biomass pyrolysis particle model: solution method optimized for the coupling to reactor models. Fuel 2012;97:80–8.
[28] Mok WSL, Antal MJ. Effects of pressure on biomass pyrolysis. 2. Heats of reaction of cellulose pyrolysis. Thermochim Acta 1983;68(2–3):165–86.
[29] Milosavljevic I, Oja V, Suuberg EM. Thermal effects in cellulose pyrolysis: relationship to char formation processes. Ind Eng Chem Res 1996;35(3):653–62.
[30] Cho JM, Davis JM, Huber GW. The intrinsic kinetics and heats of reactions for cellulose pyrolysis and char formation. ChemSusChem 2010;3(10):1162–5.
[31] Haseli Y, van Oijen JA, de Goey LPH. Numerical study of the conversion time of single pyrolyzing biomass particles at high heating conditions. Chem Eng J 2011;169:299–312.
[32] Gronli MG, Varhegyi G, Di Blasi C. Thermogravimetric analysis and devolatilization kinetics of wood. Ind Eng Chem Res 2002;41(17):4201–8.
[33] Van de Velden M, Baeyens J, Brems A, Janssens B, Dewil R. Fundamentals, kinetics and endothermicity of the biomass pyrolysis reaction. Renewable Energy 2010;35:232–42.